

**UNIVERSIDADE TECNOLÓGICA FEDERAL DO PARANÁ  
PROGRAMA DE PÓS-GRADUAÇÃO EM ENGENHARIA ELÉTRICA**

**DIERLI MAIARA DA ROSA MASCHIO**

**UMA ABORDAGEM ORIENTADA A EVENTOS PARA O  
PLANEJAMENTO DE RECURSOS EM SISTEMAS DE GERAÇÃO  
DISTRIBUÍDA DE ENERGIA**

**DISSERTAÇÃO**

**PATO BRANCO**

**2021**

**DIERLI MAIARA DA ROSA MASCHIO**

**UMA ABORDAGEM ORIENTADA A EVENTOS PARA O  
PLANEJAMENTO DE RECURSOS EM SISTEMAS DE GERAÇÃO  
DISTRIBUÍDA DE ENERGIA**  
**An Event-Driven Approach For Resources Planning In Distributed Power  
Generation Systems**

Dissertação apresentado(a) como requisito parcial à obtenção do título de Mestra em Engenharia Elétrica, do Programa de Pós-Graduação em Engenharia Elétrica, da Universidade Tecnológica Federal do Paraná.

Orientador: Prof. Dr. Marcelo Teixeira  
Coorientador: Prof. Dr. Jean Patric da Costa

**PATO BRANCO**

**2021**



[4.0 Internacional](https://creativecommons.org/licenses/by-nc/4.0/)

Esta licença permite o download e o compartilhamento da obra desde que sejam atribuídos créditos ao(s) autor(es), sem a possibilidade de alterá-la ou utilizá-la para fins comerciais.



DIERLI MAIARA DA ROSA MASCHIO

**UMA ABORDAGEM ORIENTADA A EVENTOS PARA O PLANEJAMENTO DE RECURSOS EM SISTEMAS DE GERAÇÃO DISTRIBUÍDA DE ENERGIA**

Trabalho de pesquisa de mestrado apresentado como requisito para obtenção do título de Mestra Em Engenharia Elétrica da Universidade Tecnológica Federal do Paraná (UTFPR). Área de concentração: Sistemas E Processamento De Energia.

Data de aprovação: 14 de Junho de 2021

Prof Marcelo Teixeira, Doutorado - Universidade Tecnológica Federal do Paraná

Prof Andre Eugenio Lazzaretti, - Universidade Tecnológica Federal do Paraná

Prof Dieky Adzkiya, Doutorado - Sepuluh Nopember Institute Of Technology

Prof Jean Marc Stephane Lafay, - Universidade Tecnológica Federal do Paraná

Documento gerado pelo Sistema Acadêmico da UTFPR a partir dos dados da Ata de Defesa em 14/06/2021.

À minha família e ao meu amor Rodrigo.

## ACKNOWLEDGEMENTS

Este trabalho não poderia ser terminado sem a ajuda de diversas pessoas e/ou instituições às quais presto minha homenagem. Certamente esses parágrafos não irão atender a todas as pessoas que fizeram parte dessa importante fase de minha vida. Portanto, peço desculpas àquelas que não estão presentes entre estas palavras, mas elas podem estar certas que fazem parte do meu pensamento e de minha gratidão.

A minha família, meu pai Vanilso, minha mãe Roseli, minha irmã Diulia, pelo carinho e incentivo, vocês são meus exemplos de vida.

Ao meu eterno namorado Rodrigo, pelo carinho, paciência, respeito e total apoio em minhas decisões.

A todas as amigas, em especial a Daiane e Carol pela amizade, e por estarem sempre presentes em todos os momentos da minha trajetória acadêmica e pessoal.

Aos meus orientadores, que mostraram os caminhos a serem seguidos, em especial ao professor Marcelo Teixeira que acreditou em meu potencial e não mediu esforços para me ajudar a realizar e concluir este trabalho.

A todos os professores do departamento, da banca avaliadora, e demais que ajudaram de forma direta e indireta na conclusão deste trabalho.

O cientista não é o homem que fornece as  
verdadeiras respostas; é quem faz as  
verdadeiras perguntas. (Claude Lévi-Strauss)

## ABSTRACT

MASCHIO, Dierli Maiara da Rosa. **An Event-Driven Approach For Resources Planning In Distributed Power Generation Systems**. 2021. 47 p. Dissertation (Master's Degree in Electrical Engineering) – Universidade Tecnológica Federal do Paraná. Pato Branco, 2021.

Renewable power generation systems stand as a straightforward alternative to complement the energy grid of the future. Physically, generation components have distributed nature and they work individually to supply centralised microgrids, which interface them with the main power grid and consumers. As microgrid components are non-cooperative entities, engineers are limited to plan resources consumption, fulfil unit commitments, stratify time, cost, environmental impact, quality of energy, etc. In this paper, we exploit the event-driven behaviour of microgrids to provide ways for them to recognise, communicate, and cooperate with each other towards common goals. We first design microgrids and generators as self-controlled cyber-physical agents that communicate with each other and with the main power grid. Then, we develop a Petri net simulation model that estimates customisation policies to be applied backover the microgrid via event-based control. Results show that in some cases it is possible to save effort (and resources) of power generation by replacing reactivity for a more balanced, context-aware, energy chain. A real photovoltaic plant is modelled by our approach with 86% accuracy.

**Keywords:** Microgrids. Modelling. Simulation. Control. Cooperative power generation.

## RESUMO

MASCHIO, Dierli Maiara da Rosa. **Uma Abordagem Orientada a Eventos para o Planejamento de Recursos em Sistemas de Geração Distribuída de Energia**. 2021. 47 f. Dissertação (Mestrado em Engenharia Elétrica) – Universidade Tecnológica Federal do Paraná. Pato Branco, 2021.

Os sistemas de geração de energia renovável são uma alternativa direta para complementar a rede de energia do futuro. Fisicamente, os componentes de uma microrrede têm natureza distribuída e funcionam individualmente para alimentar microrredes centralizadas, que tratam da interação com a rede elétrica principal e os consumidores. Como os componentes de uma microrrede são entidades não cooperativas, a engenharia enfrenta limitações para planejar o consumo de recursos, o cumprimento de contratos, estratificar tempo, custo, impacto ambiental, qualidade de energia, etc. Nesta dissertação, uma microrrede é explorada em relação ao seu comportamento orientado a eventos, visando o processamento desses eventos com foco no planejamento de recursos de geração. A ideia é que os componentes da microrrede reconheçam seu contexto, se comuniquem e cooperem entre si em prol de objetivos comuns. Inicialmente, microrredes e geradores são projetados como agentes ciberfísicos que se autocontrolam e se comunicam entre si e com a rede elétrica principal. Em seguida, propõe-se um modelo de simulação em redes de Petri que estima políticas de personalização para serem aplicadas sobre a microrrede, por meio de um nível de controle baseado em eventos discretos. Os resultados sugerem a possibilidade de economizar esforço e recursos de geração de energia substituindo-se a reatividade da decisão de controle por uma decisão mais equilibrada, que reconhece e pondera aspectos de toda a cadeia de energia. Uma planta fotovoltaica real é modelada por nossa abordagem com precisão de 86%.

**Palavras-chave:** Microrredes. Modelagem. Simulação. Controle. Geração de energia cooperativa.

## LIST OF FIGURES

Figure 1 – State-of-art summary and the directions taken in this paper. . . . .	13
Figure 2 – The Basic architecture of a microgrid. . . . .	15
Figure 3 – Small manufacturing system example. . . . .	17
Figure 4 – Example of a DES model, where $G = \mathcal{X} \parallel \mathcal{Y}$ . . . . .	18
Figure 5 – Example of DES control, for $K = E \parallel G$ . . . . .	18
Figure 6 – Workflow models for the manufacturing system in Fig. 3. . . . .	20
Figure 7 – Layout of the proposed framework for distributed power generation. . . . .	22
Figure 8 – Plant model Multiple-level power generator. . . . .	23
Figure 9 – Specifications multiple-level power generator. . . . .	23
Figure 10 – Plant and specification of a single-level generator. . . . .	24
Figure 11 – Plant model of a microgrid. . . . .	25
Figure 12 – A basic GSPN model for a power generator. . . . .	27
Figure 13 – Performance evaluation of a photovoltaic panel under variable resources. . . . .	30
Figure 14 – Partial layout of the real photovoltaic system at UTFPR. . . . .	32
Figure 15 – Estimated versus measured power generations . . . . .	34
Figure 16 – Proposed GSPN to design plug-and-play microgrid components. . . . .	35
Figure 17 – GSPN model for the case study. . . . .	37
Figure 18 – Storage dimensioning ( $\#R_B$ ) under three load profiles ( $\#R_L$ ): 50 to 150 tokens – 17000W to 53040W, with $\lambda_B = 1s$ . . . . .	39
Figure 19 – Storage dimensioning ( $\#R_B$ ) under three load profiles ( $\#R_L$ ): 50 to 150 tokens – 17000W to 53040W, with $\lambda_B = 0.1s$ . . . . .	40

## LIST OF TABLES

Table 1 – Input parameters derivation for $\lambda_2$ . . . . .	28
Table 2 – Plant potential and distribution. . . . .	33
Table 3 – Input parameters of the model. . . . .	33
Table 4 – Arc conditions for the microgrid model. . . . .	36

## CONTENTS

<b>1</b>	<b>INTRODUCTION</b> . . . . .	<b>11</b>
<b>2</b>	<b>LITERATURE OVERVIEW</b> . . . . .	<b>13</b>
<b>3</b>	<b>BACKGROUND</b> . . . . .	<b>15</b>
3.1	THE DISCRETE NATURE OF SYSTEMS . . . . .	16
3.2	DISCRETE EVENT SYSTEMS . . . . .	17
3.3	PETRI NETS . . . . .	19
<b>4</b>	<b>PROPOSED WORKFLOW</b> . . . . .	<b>22</b>
4.1	MODELLING AND CONTROL . . . . .	23
4.1.1	Multiple-level generation modelling . . . . .	23
4.1.2	Single-level generation modelling . . . . .	24
4.2	MICROGRID MODELLING . . . . .	24
4.3	CONTROL SYNTHESIS . . . . .	25
<b>5</b>	<b>PETRI NET-BASED CUSTOMISATION</b> . . . . .	<b>27</b>
5.1	A CASE STUDY ON PHOTOVOLTAIC GENERATION . . . . .	28
5.1.1	Photovoltaic simulation and analysis . . . . .	29
<b>6</b>	<b>CASE STUDY INVOLVING A REAL POWER PLANT</b> . . . . .	<b>32</b>
6.1	REAL SYSTEM SETUP . . . . .	32
6.1.1	Model simulation and analysis . . . . .	33
6.2	MICROGRID MODELLING . . . . .	34
6.2.1	Input parameters for M . . . . .	35
6.2.2	Microgrid simulations and analysis . . . . .	37
6.3	EXAMPLE OF COOPERATIVE DISTRIBUTION . . . . .	40
<b>7</b>	<b>CONCLUSIONS AND PERSPECTIVES</b> . . . . .	<b>42</b>
	<b>REFERENCES</b> . . . . .	<b>43</b>

## 1 INTRODUCTION

In the current model of power generation systems, a substantial amount of electricity still depends on non-renewable high-carbon sources (IEA, 2018). In recent years, however, renewable sources have appeared as an effective low-carbon way to supply the energy grid of the future (NEHRIR *et al.*, 2011). *Photovoltaic* (PV), *wind*, and *small hydroelectric* plants, for example, have shown to be sustainable alternatives. Physically, they are autonomous and distributed entities that work together to supply centralised infrastructures called *microgrids*, which also manage the interaction with the external *main power grid* (MPG) and consumers. (HATZIARGYRIOU *et al.*, 2007; LASSETER; PIAGI, 2004).

A microgrid coordinates generation, consumption, and storage, working either connected (*on-grid*) or not (*off-grid*) to the MPG (ASMUS, 2010; FARHANGI; JOOS, 2019). It is also expected to regulate its interaction with other components, protecting them from disturbances caused by its intermittent sources (MIRSAEIDI *et al.*, 2014; HARITZA *et al.*, 2016; DJELLOULI *et al.*, 2019; ZOKA *et al.*, 2004). Therefore, an important matter in microgrids is to be able to anticipate possible fluctuations that may disturb the energy supplying (JANA; CHAKRABORTY, 2020; OLIVARES *et al.*, 2014). This can be revealed, for example, by monitoring the real system. However, this option fails to provide in-advance information that could benefit planning, contingency, and predictive corrections. These steps are more impacted by modelling approaches that anticipate metrics of interest without necessarily depending on on-line systems (PAULISTA *et al.*, 2019; SIMON *et al.*, 2021).

In the literature, some modelling approaches have focused on the continuous behaviour of microgrids (PARVANIA; SCAGLIONE, 2015; JANA; CHAKRABORTY, 2020; NAVERSEN *et al.*, 2019). However, some *events* (e.g., sensing, bounds, violations) happen in a discrete manner and variations (e.g., user profile, consumption, faults) are essentially stochastic, justifying event-based complements to the continuous grid control. Event processing and simulation have been used in microgrids management (CASSETTARI *et al.*, 2017; JANA; CHAKRABORTY, 2020; TSAMPASIS *et al.*, 2016), but essentially as support for reactive actions, so that proactive planning steps are still unclear.

In this paper, event processing is exploited for predictive engineering. We show how microgrid components can be exposed as *Discrete Event Systems* (DESs) (CASSANDRAS; LAFORTUNE, 2008) that are processed both for control and optimisation. Control is handled

by using synthesis methods (RAMADGE; WONHAM, 1989) that have *Finite State Machines* (FSMs) (CASSANDRAS; LAFORTUNE, 2008) as modelling foundation. For the optimisation step, a timed *Petri Net* (KARTSON *et al.*, 1995) simulation model is proposed to discover ways for microgrid components to interact cooperatively towards common goals. Our approach can be seen as a software layer that orchestrates discrete events before triggering continuous actions in the system, taking advantages from the abstraction level in which DESs are designed and specified, and from the reconfiguration possibilities that emerge from event processing.

A real PV plant is used to illustrate and validate our approach. Initially, a single PV module is evaluated, which is then generalised for sets of modules. In both cases, the performance of the real plant is compared with estimations anticipated by our model and their proximity reveals the model's accuracy. The single-module analysis was also reproduced in *Matlab/Simulink*, using single-diode equivalent circuit model, for the sake of comparison, but the generalisation for the second analysis is not straightforward. Overall, results suggest that our approach has potential to reduce the level of uncertainties provoked by unstable power sources, by anticipating their behaviour, which make it feasible to establish cooperation policies in power generation plants.

In the following, literature and concepts are outlined in Sections 3 and 2; Section 4 introduces the architecture that will be modelled and controlled in Sections 4.1 and 5, tested in Section 6, and compared in Section 6.3. Conclusions and perspectives are shown in Section 7.

## 2 LITERATURE OVERVIEW

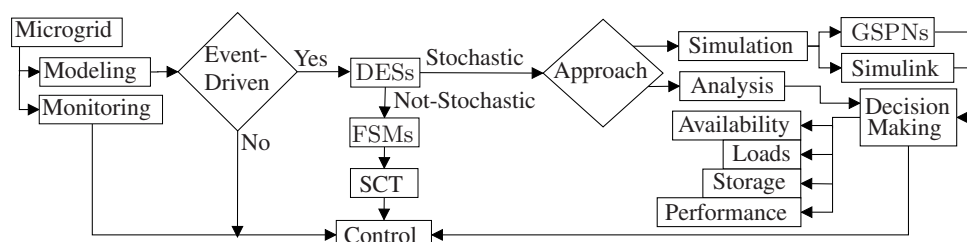
The literature related with this paper is organised as the flow in Fig. 1. Dashed lines identify related techniques not focused on this paper, while main contributions are shown otherwise.

Conceptually, reference models for microgrids are provided by benchmarks with the purpose of guiding, testing and validating their structure, whether in the design, construction or management phase (ALAM *et al.*, 2020; KOTSAMPOPOULOS *et al.*, 2018; FARHANGI; JOOS, 2019; FAN *et al.*, 2010). However, benchmarks focus on the limits (best or worst cases) of usual properties that evolve continuously in the microgrid, such as power flow, energy management, control, protection, etc. Analysis confronting probabilities and the chained impact of sporadic events in the system are, in general, neglected.

While some variables of a microgrid can be described continuously in time (PARVANIA; SCAGLIONE, 2015; NAVERSEN *et al.*, 2019), others are event-driven and require different modelling techniques and processing methods (CASSETTARI *et al.*, 2017; JANA; CHAKRABORTY, 2020; TSAMPASIS *et al.*, 2016) before they can be integrated via control. Here, the focus is on the event-driven behaviour only.

At the event level, a microgrid exposes at least two groups of events: the ones that evolve probabilistically in time, and the ones that do not. Non-probabilistic events evolve asynchronously in time, so their modelling and processing are more common using FSMs. In microgrids, FSMs have been exploited to control operation modes (SALEH *et al.*, 2017; GELEN *et al.*, 2020), transmission (RODRÍGUEZ *et al.*, 2017), storage (WANG *et al.*, 2019; VIVEIROS *et al.*, 2016), etc. In this paper, they are used to coordinate microgrid components, i.e., to estab-

**Figure 1 – State-of-art summary and the directions taken in this paper.**



Source: Author

lish the way microgrids perceive and interact with low-level components (e.g., generators) and how it interfaces them with high-level resources (e.g., MPG).

By modelling low-level (sensing, generators, resources), medium level (microgrid), and high level (MPG) components as FSMs, it is possible to process control synthesis in order to make sure that they behave as expected (SALEH *et al.*, 2017; RODRÍGUEZ *et al.*, 2017; GHASAEI *et al.*, 2020; GELEN *et al.*, 2020). Furthermore, it also becomes possible to choose certain controlled events in the system and use them as communication channels to trigger smart decisions that could make components to cooperate towards common goals. This is different from what the literature has established so far.

In this paper, cooperation policies for microgrids are discovered using simulation models that exploit the probabilistic nature of events. The modelling of probabilistic events requires resources other than ordinary FSMs. Usually, probability distributions are associated with the occurrences of events, so that they can be synchronised in time. One option is to adopt *Petri Nets* (MURATA, 1989) and their options for both simulation and state-space analysis.

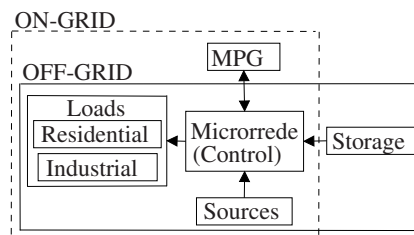
In microgrids, Petri Nets have been used for properties assessment, such as current and tension flows (LU *et al.*, 2016; CHAMORRO *et al.*, 2012; SCHOONENBERG; FARID, 2017), for availability estimation (SIMON *et al.*, 2021), and also to discover the capacity of integrated energy sources (JANA; CHAKRABORTY, 2020). In this paper, an extension of timed Petri Nets, called GSPN (KARTSON *et al.*, 1995), is adopted to complement the event-driven control with decision making capabilities. By modelling generation, storage, load, MPG, and their integrated flow, the proposed GSPN model can anticipate actions to be triggered by the event-driven controller, so that it results in a more balanced strategy for power generation.

### 3 BACKGROUND

Renewable energy sources can be exploited over the time without depleting the natural resource in use. This reduces the dependence from fossil fuels and the emissions of gases into the environment. However, their intermittent nature impacts on the power grid reliability (DENHOLM *et al.*, 2010), as the generation rate fluctuates with the resource availability, affecting the quality of energy.

One way to obtain a more balanced production is to integrate different, possibly heterogeneous, energy sources into the same grid, so that they can complement each other. Microgrid is the infrastructure that integrates different energy sources and related resources (CATALÃO, 2017; LASSETER; PIAGI, 2004), as shown in Fig. 2.

**Figure 2 – The Basic architecture of a microgrid.**



**Source: Author.**

A microgrid defines the logical link between distributed power sources, storage, MPG, and consumers (loads). It operates either *off-grid* (disconnected from the MPG), or *on-grid* (otherwise). The off-grid model usually provides *storage* resources in the form of battery banks, which can supply energy when the generation is low (CASSETTARI *et al.*, 2017). The on-grid mode is connected with the MPG, which allows either to complement the generation profile, or to inject surplus, as convenient.

However, the intermittent nature of microgrids cause adverse scenarios to the continuous power delivering. For example, in long rainy periods, PV generation reduces considerably and in case this source is predominant, electricity may become scarce. Other adversities are peak consumption, low level storage, or even failures that may cause discontinuity (SIMON *et al.*, 2021).

These features can be handled, to some extent, by observing the behaviour of the microgrid and *identifying* a system of equations that describe variables such as frequency, power, and voltage. By manipulating those variables, the microgrid can then be controlled with consid-

erable precision. A grid can also be observed from an event-driven view, which reveals different variables such as performance, failures, spikes, interruptions, availability, and load profile. In general, these variables cannot be directly equated, as they behave unpredictably in time. When both continuous and discrete variables are observed into the same application domain, e.g., a *self-healing* system, it is said to be *hybrid* (CASSANDRAS; LAFORTUNE, 2008).

**Example 1.** Consider a self-Healing system (ZANGENEH; MORADZADEH, 2020) that restores the energy autonomously and as quickly as possible after a failure report. It identifies the failure, isolates it, and recovers the system. Part of these actions (e.g. interruption, isolation, and healing processing) are event-driven, while other part (e.g. the active control itself) is continuous and depends on the triggered events.

Although the hybrid nature of a microgrid can be exploited in different ways (ZHANG *et al.*, 2019; DADFAR *et al.*, 2019; PATHAK; YADAV, 2019), it is in the following exposed as a *Discrete Event System* (DES) (CASSANDRAS; LAFORTUNE, 2008), and the focus is centred on the events that may disturb the system. After appropriate event processing, DESs can result in valuable information and tools for predictive engineering (PAULISTA *et al.*, 2019; RUPNIK *et al.*, 2020).

### 3.1 THE DISCRETE NATURE OF SYSTEMS

In the hierarchy of dynamic non-linear systems, there is a major feature that defines the way a system can be observed, modelled, and controlled: its dependency on *time*. In time-dependent systems, states change as time changes. Their model usually arises from equations that take time into account, and their control consists of manipulating variables over the time. Differently, time-independent systems evolve asynchronously in time, so that equations become inappropriate to describe their behaviour. *Discrete Event Systems* (DESs) (CASSANDRAS; LAFORTUNE, 2008) are examples of time-independent behaviours. DESs are more naturally modelled by diagrams that map their trajectories over the state-space upon observing the occurrence of events. Although a system may include hybrid features, it is the event-driven view that facilitates engineers to comprehend and handle complex chains of events logically, with a high level of abstractions. Within the event-driven class of dynamic systems, there are further two sub classes that refer to the nature of occurrence of events in a DES, which can be either *deterministic*, or *stochastic* (CASSANDRAS; LAFORTUNE, 2008). In this paper, deterministic

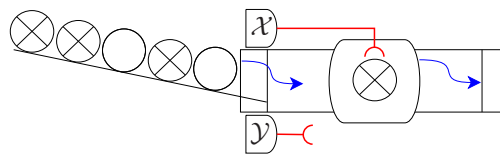
events are exploited in control, while stochastic events are exploited for the purpose of customisation. In the following, we present two approaches that are used in the paper to deal with both types of events.

### 3.2 DISCRETE EVENT SYSTEMS

Many real-world systems are event-driven, such as robotics and manufacturing. In particular, they cannot be described by simply equating their phenomena on time, but by mapping their asynchronous signals, called *events*, at discrete points of the time, which forms a well-defined enumerable set of states.

**Example 2.** As an example of event-driven systems, consider a small manufacturing system where two robots,  $\mathcal{X}$  and  $\mathcal{Y}$ , process two types of workpieces, as shown in Fig. 3.

**Figure 3 – Small manufacturing system example.**



Source: Author

Robot  $\mathcal{X}$  is supposed to process only workpieces type 1, while  $\mathcal{Y}$  processes workpieces type 2. When seen as a DES, it is of interest to observe the events that lead the robots to manufacture workpieces properly, such as *start* and *finish* commands, and in which logic ordering. The interval between occurrences of events is neglected in DESs. Remark that the system in Fig. 3 includes variables that evolve continuously in time (e.g., strength, speed, and pressure to move the robot arm). However, those variables are not considered when the system is seen as a DES. The observation, here, is focused on the signals that lead to trigger those continuous variables (e.g., *start* and *finish* moving the arms), which can be modelled as follows.

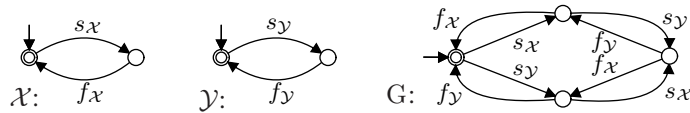
Formally, a DES can be exposed as a *Finite State Machine* (FSM) modelled as a tuple  $M = (\Sigma, Q, q^\circ, Q^m, \rightarrow)$  that includes: a set  $\Sigma$  of symbols denoting events; a set  $Q$  of states, with an initial state  $q^\circ \in Q$ ; a subset  $Q^m \subseteq Q$  of marked (or final) states, used to express complete tasks; and finally a transition set  $\rightarrow \subseteq Q \times \Sigma \times Q$  that models the system migrating from a state  $q_1$  to another,  $q_2$ , when an event  $\sigma$  occurs, which is graphically denoted by  $q_1 \xrightarrow{\sigma} q_2$ .

When modelling DESs as FSMs, the ability to combine models, forming larger systems, allows engineers to avoid design complexity. Two FSMs  $A = (\Sigma_A, Q_A, q_A^\circ, Q_A^m, \rightarrow_A)$  and

$B = (\Sigma_B, Q_B, q_B^o, Q_B^m, \rightarrow_B)$  can be *composed* (CASSANDRAS; LAFORTUNE, 2008), notation  $A \parallel B$ , such that events shared between  $A$  and  $B$  are forced to occur simultaneously, while the others occur in any order.

**Example 3.** Components in Fig. 3 are modelled in Fig. 4.

**Figure 4 – Example of a DES model, where  $G = \mathcal{X} \parallel \mathcal{Y}$ .**



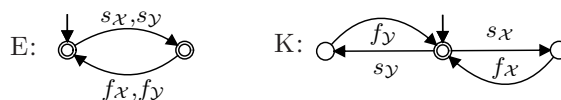
Source: Author

FSMs  $\mathcal{X}$  and  $\mathcal{Y}$  model start and finish events for the robot arms, while  $G = \mathcal{X} \parallel \mathcal{Y}$  exposes graphically their composition. In the initial state, both  $\mathcal{X}$  and  $\mathcal{Y}$  are able to start operating. This is reasonable when components are seen individually but, in conjunction,  $\mathcal{X}$  and  $\mathcal{Y}$  are expected to work under coordination. This is approached next.

Then, a DES modelled as a composition of FSMs can be specified to result in the sequence of events expected under control. Specifications can also be designed as modular FSMs and composed to the system model to control it.

**Example 4.** Fig. 5 specifies the DES plant in Fig. 4.

**Figure 5 – Example of DES control, for  $K = E \parallel G$ .**



Source: Author

Model  $E$  implements mutual exclusion on  $\mathcal{X}$  and  $\mathcal{Y}$ . It allows either  $\mathcal{X}$  or  $\mathcal{Y}$  to start, however, upon starting, the other is prevented to also start until the first finishes. The mutual exclusion effect is revealed graphically in  $K = E \parallel G$ .

Let  $G = \parallel_{j=1}^m G_j$  and  $E = \parallel_{i=1}^n E_i$  be FSMs modelling, respectively, a DES and its specifications. The composition  $K = G \parallel E$  models the behaviour of the system under control, as projected by the engineer. However,  $K$  assumes that any events in  $G$  is subject to control, while in practice some events can be *uncontrollable*. Not considering their differences may violate the control consistency, situation when the controller commands a certain action that cannot be reproduced physically. Sensor signals, communication breakdowns, and signal dropouts, for

example, are events that occur uncontrollably. In Fig. 4, events  $f_x$  and  $f_y$  are uncontrollable. They are observable and expected to occur, but cannot be handled in advance by the controller.

Formally, controllability can be presented by partitioning the set of events  $\Sigma = \Sigma_c \cup \Sigma_u$  into *controllable* ( $\Sigma_c$ ) and *uncontrollable* ( $\Sigma_u$ ) events. Then, those partitions can be mathematically exploited to extract from  $K$ , a maximal sub-model that respects the impossibility of disabling events in  $\Sigma_u$ . In *Supervisory Control Theory* (RAMADGE; WONHAM, 1989), this computation is called *control synthesis* and the result is classically called the *supremal* or *optimal* controller, in the sense that it is controllable, least restrictive, and non-blocking.

In this paper, optimal controllers are synthesised from generators, microgrids, surrounding devices, and related specifications. They form the (exact) event-driven layer of software for microgrids. Upon communication (not approached here), microgrids components can cooperate, as long as they recognise the context of each other. Cooperation policies are pursued in this paper by means of *Petri Net* simulation model, discussed next.

### 3.3 PETRI NETS

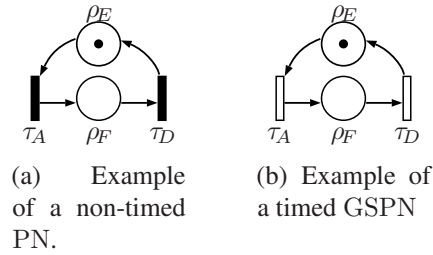
*Petri net* (PN) (MURATA, 1989) is a modelling formalism that allows expressing and evaluating properties of DESs. While its external layout is similar to fluxograms, facilitating visual inspection, internally it has a solid mathematical foundation that allows formalising several properties of DESs.

Structurally, a PN can be seen as a directed graph composed of *places*, *transitions*, and directed *arcs* (connecting places and transitions). To express states, and conditions holding in a given state, places are marked with *tokens*. The state of a PN changes when a transition fires, moving tokens from input to output places through arcs. A transition can fire if it is *enabled*, i.e., if its input places have enough tokens for the arcs to take. Furthermore, firing may depend on a probabilistic rule or on the priority associated with the transition.

**Example 5.** Consider the manufacturing system in Fig. 3. Workpieces are delivered to a conveyor and moved to a static desk, for assembling with the robot  $\mathcal{X}$  or  $\mathcal{Y}$ . The PNs in Fig. 6 design workpieces flowing through the assembly desk.

Each model has two places,  $\rho_E$  and  $\rho_F$ , modelling respective the desk empty and full. Transitions  $\tau_A$  and  $\tau_D$  model events of sensors signalling respectively arrivals and departures of workpieces. In the initial state, the system is empty, therefore  $\rho_E$  is marked, and  $\rho_F$  is marked

Figure 6 – Workflow models for the manufacturing system in Fig. 3.



Source: Author

otherwise. The difference between figures 6(a) and 6(b) is that 6(b) considers the delay taken by a workpiece to arrive and leave the system.

Some extensions of PNs have been developed to include time and probability to transitions. This allows the design of other classes of DESs that evolve accordingly. *Generalised Stochastic Petri Nets* (GSPNs) (KARTSON *et al.*, 1995), for example, represent *time* by either deterministic or exponentially distributed *variables* associated to *timed transitions*, combined to *non-timed* (or *immediate*) transitions (DESROCHERS, 1994). Formally, a GSPN is a 7-tuple  $\mathcal{N} = \langle \mathcal{P}, \mathcal{T}, \Pi, I, O, M, W \rangle$ , where:

- $\mathcal{P} = \{\rho_1, \rho_2, \dots, \rho_n\}$  is a finite set of places;
- $\mathcal{T} = \{\tau_1, \tau_2, \dots, \tau_n\}$  is a finite set of transitions;
- $\Pi : \mathcal{T} \rightarrow \mathbb{N}$  is the priority function, where:

$$\Pi(\tau) = \begin{cases} \geq 1, & \text{if } \tau \in \mathcal{T} \text{ is an immediate transition;} \\ 0, & \text{if } \tau \in \mathcal{T} \text{ is a timed transition.} \end{cases}$$

- $I : (\mathcal{T} \times \mathcal{P}) \rightarrow \mathbb{N}$  is the input relation that defines arcs connecting places to transitions;
- $O : (\mathcal{T} \times \mathcal{P}) \rightarrow \mathbb{N}$  is the output relation that defines arcs connecting transitions to places;
- $M : \mathcal{P} \rightarrow \mathbb{N}$  maps the initial marking, i.e., the amount of tokens in each place  $\rho \in \mathcal{P}$ . Marking of  $\rho$  is denoted  $\# \rho$ ;
- $W : \mathcal{T} \rightarrow \mathbb{R}^+$  is the weighting function that represents either a weight ( $w_\tau \in \mathbb{N}$ ), or a delay ( $\lambda_\tau \in \mathbb{R}$ ), such that:

$$W(\tau) = \begin{cases} w_\tau \geq 0, & \text{if } \tau \in \mathcal{T} \text{ is immediate;} \\ \lambda_\tau > 0, & \text{if } \tau \in \mathcal{T} \text{ is timed.} \end{cases}$$

The trajectory through the state-space of  $\mathcal{N}$  depends on the *pre* and *post* conditions of each transition  $\tau$ , defined respectively by the sets  $\overleftarrow{\tau} = \{\rho \in \mathcal{P} \mid I(\tau, \rho) > 0\}$ , and  $\overrightarrow{\tau} = \{\rho \in \mathcal{P} \mid O(\tau, \rho) > 0\}$ ;  $\tau$  is said to be *enabled* in a marking  $M$  if, and only if,  $\forall \rho \in \overleftarrow{\tau}, M(\rho) \geq I(\tau, \rho)$ .

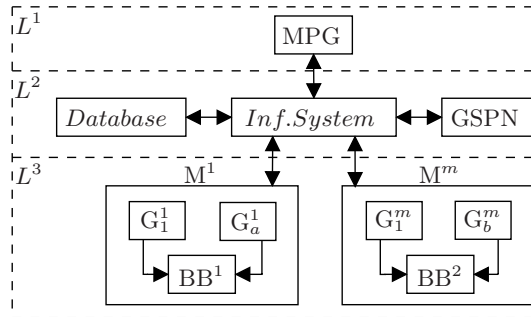
Therefore, a state of  $\mathcal{N}$  changes when enabled transitions *fire*, and only they can fire. *Immediate* transitions fire as soon as they get enabled, while *timed* transitions wait for a delay  $\lambda_\tau$ , that can be either deterministic ( $\lambda_{d\tau}$ ), or stochastic ( $\lambda_{s\tau}$ ), in this case associated with an exponentially distributed delay. Delays of timed transitions are inversely proportional to the frequency of firing, relation that defines the so-called *firing rate*. Timed transitions are additionally associated with a *serverType* that defines the way multiple customers are handled. *Infinite* server allows to attend tokens concurrently, while *single* server implies a sequential processing.

An important feature of  $\mathcal{N}$  is being *bounded*. When a transition fires, it moves tokens from input to output places. Therefore, the firing of  $\tau \in \mathcal{T}$ , enabled in the marking  $M$ , causes a new marking  $M'$  such that  $\forall \rho \in (\overleftarrow{\tau} \cup \overrightarrow{\tau}), M'(\rho) = M(\rho) - I(\tau, \rho) + O(\tau, \rho)$ .  $\mathcal{N}$  is said to be *bounded* if it allows a finite number  $k > 0$  of tokens in each place, ensuring a resulting finite state-space.

When compared to other state-space-based approaches, such as *Markov Chains*, GSPNs are shown to be more general, as they support either simulation or state-space analysis. Furthermore, GSPNs allow to combine exponential transitions to form more complex time distributions (DESROCHERS, 1994), broadening its applicability over DES problems.

## 4 PROPOSED WORKFLOW

Figure 7 – Layout of the proposed framework for distributed power generation.



Source: Author

Consider the 3-layers workflow in Fig. 7.  $L^1$  represents the external main power grid from where generation requests arrive periodically.  $L^2$  receives those requests and dispatches the generation plan in  $L^1$ , using an information system that also integrates data storage, optimisation modules, and interface.

It is assumed that the layer  $L^3$  includes a finite number  $j = 1, \dots, m$  of microgrids  $M^j$ , each one supporting a finite number of generators  $G_i^j$ ,  $i = 1, \dots, g$ , such as *wind*, *photovoltaic*, *biomass*, *thermal*, and *small hydropower plants* (SHPs). Furthermore, each microgrid  $M^j$  may integrate a battery bank  $BB^j$ , for energy storage. Microgrids  $M^j$  manipulate and report to the other levels variables such as frequency, voltage, power, and resources availability.

Energy storage is important because it allows balancing variations in the renewable production, in addition to covering the uncertainties in generation and consumption. With the use of a battery bank, the system operator can implement load shifting, improve voltage and frequency stability, reduce peak load, improve power quality, and postpone system updates (BIAZARGHADIKOLAEI *et al.*, 2019). Therefore, the ability to anticipate energy storage conditions and their correlations are crucial for power systems planning.

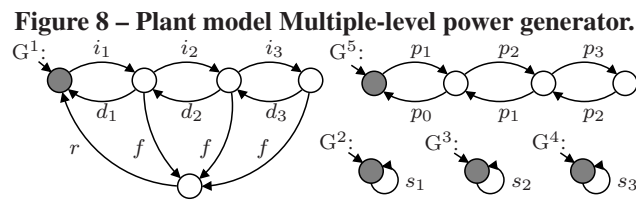
In the next section, design and control of each layer is developed using supervisory control. Then, we implement and communicate the elements through the layers for them to cooperate based on policies to be further derived in Section 5.

## 4.1 MODELLING AND CONTROL

Seen as DESs, power generators can be of two types: the ones which controllably deliver multiple levels of power (e.g., hydroelectric), and the ones which generate power according to the uncontrollable availability of resources (e.g., *wind* and *sun*). These two classes are modelled as follows.

### 4.1.1 Multiple-level generation modelling

The plant of a multiple-level power generator is formed by: a  $k$ -level generator,  $k$  sensors, and a  $k$ -level power demand *prescriber*. For illustration,  $k$  is limited to 3, but this can be straightforwardly extended to any finite number. The plant model of a generator is shown in Fig. 8.

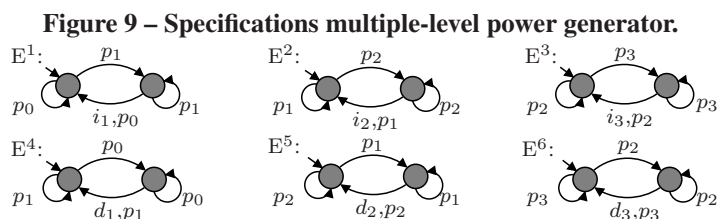


Source: Author

The FSM  $G^1$  models the generator;  $G^2$ ,  $G^3$ , and  $G^4$  are associated with signals provided by *sensors* that report resources levels (e.g., water); and  $G^5$  models a power demand *prescriber*, responsible for interfacing the generation level with the microgrid control.

Events  $i_t$  and  $d_t$ , for  $t = 1, 2, 3$ , *increase* and *decrease* the generation level  $t$ ; events  $f$  and  $r$  model *fault* and *recovery* of  $G^1$ ;  $p_t$ , for  $t = 0, 1, 2, 3$ , represents the power *prescription*; and  $s_t$ , for  $t = 1, 2, 3$ , indicates the *sensed* level of resources. It is assumed that  $\Sigma_c = \{i_t, d_t, r\}$  and  $\Sigma_u = \{p_t, f, s_t\}$ .

For the purpose of control, the specifications are:



Source: Author

- $E^{1,2,3}$ : avoid starting the generation levels  $i_{1,2,3}$  while there is no corresponding prescription from  $p_{1,2,3}$ ;
- $E^{4,5,6}$ : avoid reducing the generation levels  $d_{3,2,1}$  while not prescribed from  $p_{2,1,0}$ .

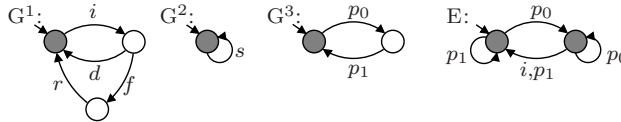
Fig. 9 shows the specification models. For example,  $E^2$  prohibits the event  $i_2$  (66.6% of the total plant potential) unless it is explicitly prescribed (event  $p_2$ ) by the microgrid. The same reasoning applies for the others.

#### 4.1.2 Single-level generation modelling

Some plants, such as *wind* and *photovoltaic*, produce power under a single-level mode that depends on the uncontrollable variation of resources, so that the controller can only decide whether generating power or not.

To design this type of generator, it has been considered: a *sensor* for detecting resources variability (such as wind level and solar irradiation); a *generator*; and a *demand prescriber*. They are modelled as in Fig. 10.

**Figure 10 – Plant and specification of a single-level generator.**



Source: Author

FSM  $G^1$  models *on* (event  $i$ ) and *off* (event  $d$ ) generation modes, also considering *failures* (event  $f$ ) and *recovery* (event  $r$ ); FSM  $G^2$  designs the sensor, which identifies resources availability (event  $s$ ); and FSM  $G^3$  models the power prescriber by identifying whether (event  $p_1$ ) or not (event  $p_0$ ) there exists external demand for power generation. It is assumed that  $\Sigma_c = \{i, d, r\}$ , while  $\Sigma_u = \{p_0, p_1, f, s\}$ .

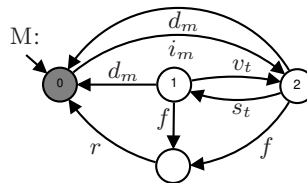
The control consists in coordinating generator and prescriber, i.e., starting the production only when requested so, and preventing it to stop while there is still an active request. The FSM  $E$  designs this rule in Fig. 10.

## 4.2 MICROGRID MODELLING

The microgrid interacts with both multiple and single level generators. The amount of energy produced by the microgrid is, therefore, given by the sum of all portions received from

the associated generators. A microgrid model is shown in Fig. 11.

**Figure 11 – Plant model of a microgrid.**



**Source: Author**

Events  $i_m$  and  $d_m$  model the start and stop of the microgrid;  $f$  and  $r$  model fault and recovery;  $vt$  means the arrival of a prescription from the MPG; and  $st$  means that the microgrid has been set up for the prescription  $vt$ . It is assumed that  $\Sigma_c = \{d_m, i_m, st, r\}$ , while  $\Sigma_u = \{vt, f\}$ .

Upon starting (transition  $0 \xrightarrow{i_m} 2$ ), the microgrid sets up the production according to its current *prescription*, which is initially empty. The conclusion of the set up is signaled by the event  $st$ , which evolves the microgrid to the state 1 where it waits for any variation of the prescription coming from the MPG. When it does (event  $vt$ ), the microgrid returns to the state 2 and starts the production accordingly. This is achieved by sending an actuation instruction to the generators under the microgrid, describing the amount of energy expected to be generated by each of them.

The actuation scheme can be computed in such a way that it balances arguments such as: (i) the level of resources reported by each generator; (ii) the power capacity of each generator; (iii) the priority of use, which can be defined, for example, according to green policies; and (iv) the time available to fulfil the demand in contrast with the number of generators and their capacity. Later, in Section 5, we show a method to calibrate the actuators.

### 4.3 CONTROL SYNTHESIS

Let a microgrid be modelled by  $M^1$  with 4 states as in Fig. 11, under which two generators operate. The first is of the type multiple-level and it is modelled by the plant  $G_1^1 = \parallel_{p=1}^5 G^p$  (Fig. 8), specified by  $E_1^1 = \parallel_{q=1}^6 E^q$  (Fig. 9). Then, for  $K_1^1 = G_1^1 \parallel E_1^1$ , the controller  $\text{supC}(K_1^1, G_1^1)$  is modelled by  $V_1^1$  with 105 reachable states.

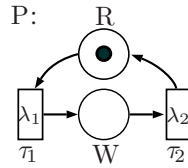
The second generator is single-level type and it has plant  $G_2^1 = \parallel_{p=1}^3 G^p$  and specification  $E_2^1 = E$  as in Fig. 10. For  $K_2^1 = G_2^1 \parallel E_2^1$ , the controller  $\text{supC}(K_2^1, G_2^1)$  is modelled by  $V_2^1$  with 9 states.

$M^1$ ,  $V_1^1$ , and  $V_2^1$  can then be translated to implementable code and deployed in hardware, e.g., a microcontrolled system. Each controller ( $V_1^1$  and  $V_2^1$ ) can be further communicated with  $M^1$ , according to the workflow in Fig. 7, so that they can report their status and receive customised prescriptions for power generation, which is approached next.

## 5 PETRI NET-BASED CUSTOMISATION

In addition to the event-based control, elements of a microgrid are expected to cooperate toward common goals. In this paper, cooperation policies are discovered by simulating GSPNs that model power generators. A GSPN that represents a general power generator is shown in Fig. 12.

**Figure 12 – A basic GSPN model for a power generator.**



**Source: Author**

P is composed of two places, R and W, connected by the timed transitions  $\tau_1$  and  $\tau_2$ . R quantifies the *resources* (tokens) available for power generation, while W models the *working* place, i.e., energy production.  $\tau_1$  and  $\tau_2$  impose state transitions to P using tokens in R and W, and *firing* delays.

Transition  $\tau_1$  fires at a rate  $1/\lambda_1$ , in which  $\lambda_1$  is its *delay*.  $\tau_2$  has a firing rate of  $1/\lambda_2$ , for a delay  $\lambda_2$  representing the time took by the generator to produce a given portion of energy. Here,  $\#R$  is set to 1 in order to model generators producing sequentially, one energy unit at a time, after a delay  $\lambda_2 \geq \lambda_1$ . Later, multiple generators are designed and ( $\#R$ ) is set accordingly. Also, it has been assumed a *Single Server* firing policy for  $\tau_2$  (see Section 3.3), while later this may have to be replaced by the *Infinite Server* policy.

From P, multiple generation profiles can be reproduced by simply varying  $\lambda_2$ , or by setting workflows that connect multiple P models. This allows to capture distinct plant profiles and environmental changes, such as panel shading or wind intensity, when it is the case. Remark that these events are reported by the sensors that follow generators in the level  $L^3$  of Fig. 7. They are used to calculate the parameters for  $\lambda_2$ , as follows:

$$\lambda_2 = \frac{\Delta R_M}{(R_M - \min(R_M))} \cdot T, \quad (1)$$

where  $\Delta R_M = \max(R_M) - \min(R_M)$  defines the range of resource level within which the generator can produce;  $R_M$  is the real (measured) *resource*; and  $T$  is the observation interval. By

feeding  $P$  with different values for  $\lambda_2$ , one can simulate, for example, photovoltaic generation, as exploited next.

### 5.1 A CASE STUDY ON PHOTOVOLTAIC GENERATION

The basic principle of PV technology is to use *solar radiation* ( $S$ ) over panel cells to generate electrical current (VILLALVA *et al.*, 2009). However, there are many variables involved in this process that interfere on the power generation performance (KING *et al.*, 1997). For example, the incidence of  $S$  is variable; each panel has a constant capacity; panels can be clustered differently; each part of a power plant can receive different rate of  $S$ ; etc.

Therefore, when applying  $P$  as in Fig. 12 to model a *solar* panel (denote  $P^S$ ), these variables have to be considered. In the model that follows, they are used only to calculate the delay  $\lambda_2$ . When a token is in  $R$  waiting  $\tau_1$  to fire, this means the absorption of solar radiation over the panel, which here is assumed to be immediate, so  $\lambda_1$  is set to 1. When the token moves to  $W$  and waits  $\tau_2$  to fire, after a delay  $\lambda_2 \geq \lambda_1$ , this means the time took by the panel to generate a given portion of energy as a function of variable solar incidence indexes. Therefore,  $\lambda_2$  can be calculated as in Eq. (1), for  $R = S$ . The result is the set of input parameters presented in Tab. 1, which can be used to feed a GSPN  $P^S$  and vary  $\lambda_2$ .

**Remark 1.** As  $\lambda_2$  may change very frequently as a function of the solar incidence, the mean amount of energy produced within a certain period of time is unclear from the panel specification, benchmarks or analytic processing. Thus, our intention here is to anticipate power generation under variability, specially in the context of a more general microgrid system as in Section 6.

**Table 1 – Input parameters derivation for  $\lambda_2$ .**

Hour	$S (W/m^2)$	$\lambda_2 (s)$	Hour	$S (W/m^2)$	$\lambda_2 (s)$
10:00	190.81	9.9108	16:00	1005.83	1.0
11:00	401.94	2.9807	17:00	900.56	1.0106
12:00	716.94	1.4588	18:00	725.00	1.4400
13:00	890.28	1.1388	19:00	401.67	2.9834
14:00	1004.17	1.0	20:00	149.08	18.3374
15:00	1043.89	1.0			

Tab. 1 uses an illustrative sample of solar radiation collected from a meteorological station in Brazil. The second column presents the radiation ( $S$ ) measured for each period under observation (first column), while the third column shows the time, in seconds, to be assigned to

$\lambda_2$  to represent the panel production under the corresponding radiation  $S$  (calculated as in Eq. (1)). As the whether conditions are good, the generation is expected to reach the full potential of the PV panel.

**Remark 2.** In Tab. 1, the greater the delay  $\lambda_2$ , the fewer the amount of generated power, and the longer the time to generate it. For example, at 10 o'clock,  $S = 190.81W/m^2$  requires  $9.9108s$  to generate the same amount of energy produced at 14 o'clock within  $1s$ . Between 14 and 16 the system reaches the maximum potential, which is bounded by the panel capacity.

For illustration, assume that  $P^S$  is a panel that generates  $330W$  (Watts) per second ( $1s$ ) under maximum  $S$  rate ( $max(S)$ ) and under mean temperature of  $25$  Celsius degrees. The acceptable range for photovoltaic production is between  $min(S) = 100W/m^2$  and  $max(S) = 1000W/m^2$ , which gives  $\Delta S = 900W/m^2$ . Assume also that  $T$  is associated with  $1s$ , meaning the immediate generation of the panel full power. When  $S \geq 1000$ , the delay  $\lambda_2$  is set to  $min(\lambda_2) = 1$ , which returns the maximum performance production. Also  $\lambda_1$  is set to  $min(\lambda_2)$ , as one aims to observe variations in  $\lambda_2$  only.

The following question can now be introduced.

**Question 1.** Consider a panel with maximal performance  $max(S)$  is  $350W$  each  $1s$ . By making  $\lambda_2 = 1$ , the value of each token after  $\lambda_2$  is  $350W$ . However, any variation of  $S$  makes  $1s$  no longer enough to generate  $350W$  and one wonders either what is the amount of energy generated within the same  $1s$ , or when will the system be able to generate  $350W$  under variable  $S$ .

Model  $P^S$  can then be simulated to answer this type of question, as follows.

### 5.1.1 Photovoltaic simulation and analysis

After feeding the model  $P^S$  with the parameters in Tab. 1, it is simulated to compute metrics of interest. All simulations in this paper use the *Stationary Simulation Standard* algorithm implemented by the *TimeNet* tool (ZIMMERMANN; KNOKE, 2007), considering a confidence level of 95%, and relative error of 10%.

Then,  $\tau_2$  was increasingly varied to estimate the system *utilisation*:

$$\mathcal{U}(W) = (\#W \geq 0), \quad (2)$$

meaning the probability of how busy the system is likely to be; and the system *response time*:

$$\mathcal{R}(W) = (\mathcal{E}(W)) \cdot (1/\lambda_2), \quad (3)$$

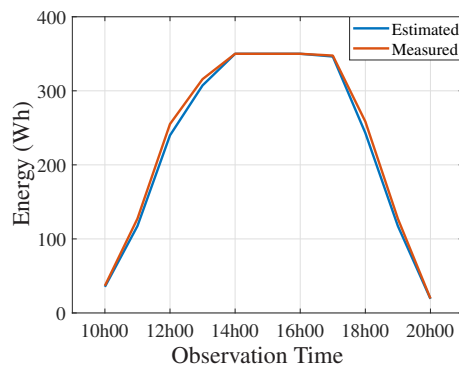
meaning how long the system takes to produce certain amount of energy, for

$$\mathcal{E}(W) = (\#W), \quad (4)$$

capturing the mean *expectation* of marking in the place  $W$ , and  $\mathcal{R}$  confronting this expectation further with the frequency of firing, which returns the mean waiting time in  $W$ .

By using the formula  $\mathcal{R}(W)$ , one can provide answers for the Question 1, as it maps the performance estimated for a PV panel when operating under variable incidence of resources. It remains to know whether this estimation coincides with the performance that would result from the real panel. In Fig. 13, the real performance is obtained from the panel specification, but later, in Section 6, it will be measure directly from the real installed system.

**Figure 13 – Performance evaluation of a photovoltaic panel under variable resources.**



When  $S \geq 1000W/m^2$  (between 14 and 16 o'clock), both estimation and specification suggest the full  $350W$  generation within  $1s$ . However, the performance is of only  $35.3W$  (real) and  $36.8W$  (estimated) when  $S = 190.81W/m^2$ ; improving to  $243.1W$  (real) and  $259.7W$  (estimated) when  $S = 725W/m^2$ .

Other perspective for Question 1 is: which is the amount of energy estimated to be obtained between 11 and 12 o'clock, which turns out to be  $128.4W$ . One may also wonder how long the system takes to generate  $1000W$ , if  $S$  is  $401.94W/m^2$ , for which simulation informs  $2.9807s$ .

With these estimations on hands, the control level  $L^2$  can be informed whether or not the available microgrids can reach the target production, and whether or not a new dispatch plan is needed for the microgrids. The advantage of having these information in advance is

that reconfiguration can be done preventively, without the need for measuring the real system. Measures tend to be more precise in comparison with simulations, but they allow only for reactive engineering, while simulations project predictive engineering.

The estimations in Fig. 13 have accuracy of 95.9% with respect to the real system behaviour. This suggests that the model can now be extended and tested under more complex, variable, and larger scenarios. In the following, the model is tested in the context of a real plant. A single panel is again used as the basic evaluation, which is then extended to a set (string) of combined panels. Other components inside a microgrid are also integrated to the model, such as storage facilities, loads, and external power supplier.

## 6 CASE STUDY INVOLVING A REAL POWER PLANT

This section applies our model to determine the performance of a real PV plant. Section 6.1 presents the system setup, which is assessed first as a group of panels in Section 6.1, and as a microgrid in Section 6.2. Simulation results for both scenarios are respectively discussed in sections 6.1.1 and 6.2.2.

### 6.1 REAL SYSTEM SETUP

**Figure 14 – Partial layout of the real photovoltaic system at UTFPR.**



**Source: UTFPR.**

The following experiments are conducted over a  $420kW$  photovoltaic system installed at the *Federal University of Technology Paraná (UTFPR)*, in Brazil. The plant is composed of 1237 panels distributed over different block buildings. The panels of each block form strings that are connected to 7 inverters that transform continuous to alternate power. Each string is linked to a *Maximum Power Point Tracker (MPPT)*, responsible for maintaining the power coming from the panel, through the current control. For the sake of brevity, a single inverter was chosen for illustration. It is composed of 8 strings of panels, 156 panels in total of  $340W$  each, as shown in Tab. 2.

The irradiation data, obtained from the sensors positioned close to this inverter, are used to derive (by the Equation (1)) the input parameters for the GSPN model in Fig. 12. The collected data can be found in Tab. 3.

**Table 2 – Plant potential and distribution.**

MPPT ID	String ID	Number of panels	Capacity (W)
MPPT 1	F - 1	22	7480
	F - 2	22	7480
MPPT 2	F - 3	17	5780
MPPT 3	F - 4	22	7480
	F - 5	22	7480
MPPT 4	F - 6	17	5780
	F - 7	17	5780
MPPT 5	F - 8	17	5780
TOTAL		156	53040

**Table 3 – Input parameters of the model.**

Hour	S(W/m <sup>2</sup> )	$\lambda_2$ (s)	Hour	S(W/m <sup>2</sup> )	$\lambda_2$ (s)	Hour	S(W/m <sup>2</sup> )	$\lambda_2$ (s)
07:30	181.4	11.0565	11:00	778.3	1.3268	14:15	757.9	1.3680
07:45	185.5	10.5263	11:15	794.0	1.2968	14:30	189.6	10.0446
08:00	220.0	7.5000	11:30	806.4	1.2741	14:45	635.6	1.6804
08:15	347.8	3.6320	11:45	814.4	1.2598	15:00	649.4	1.6382
08:30	404.0	2.9605	12:00	817.7	1.2540	15:15	586.4	1.8503
08:45	427.5	2.7481	12:15	812.7	1.2628	15:30	507.6	2.2080
09:00	475.4	2.3974	12:15	812.7	1.2628	15:45	461.5	2.4896
09:15	530.9	2.0887	12:30	802.9	1.2804	16:00	240.7	6.3966
09:30	572.2	1.9060	12:45	800.2	1.2853	16:15	488.0	2.3196
09:45	616.1	1.7438	13:00	793.3	1.298	16:30	425.8	2.7624
10:00	660.5	1.6057	13:15	793.7	1.2974	16:45	332.0	3.8793
10:15	694.3	1.5144	13:30	350.3	3.5957	17:00	258.2	5.6890
10:30	726.5	1.4366	13:45	776.6	1.3302	17:15	167.0	13.4328
10:45	756.9	1.3701	14:00	767.1	1.3491	17:30	121.8	41.2844

### 6.1.1 Model simulation and analysis

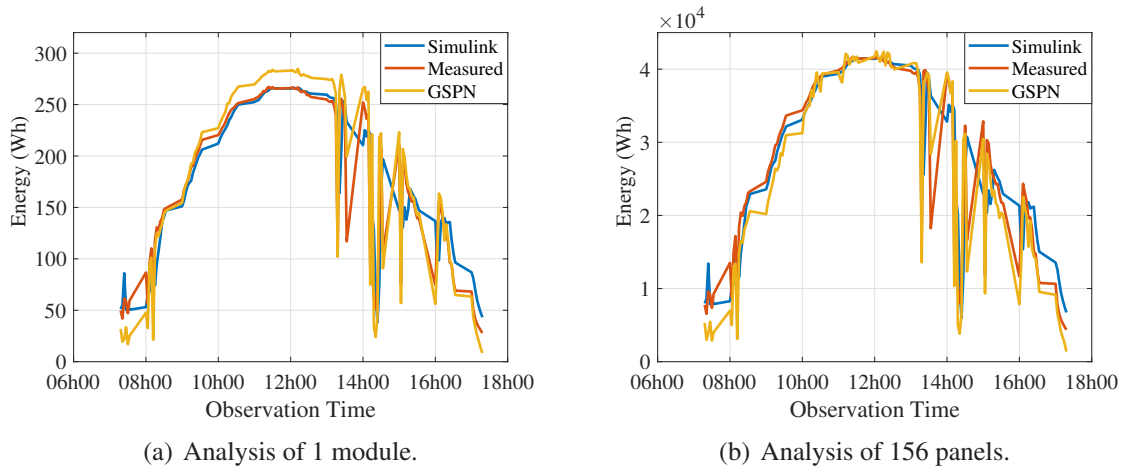
The model is then simulated to anticipate the performance possibly achieved by the panels when in production under variable resources. The simulations were further separated into the three steps that follow:

- (i) The panel performance is estimated using the GSPN model;
- (ii) The real performance resulting from the inverter containing the 156 panels is measured in the real plant;
- (iii) The dynamic generation system is further reproduces for comparison using the *Matlab Simulink* Toolbox.

The samples are then compared and Fig. 15 shows the results.

Inspection shows that the performance estimated by the GSPN model has a proximity of 86% with respect to the real plant performance, in both tests, while the Simulink/Matlab model returns a proximity of 81% compared to the real system. The formula used to approxi-

**Figure 15 – Estimated versus measured power generations**



mate the curves is accuracy:

$$E = \frac{x_m - x_e}{x_m}, \quad (5)$$

in which  $x_m$  is the measured, and  $x_e$  is the estimated (GSPN and Simulink) values. The result of Eq. (5) are deducted from 100%, leading to the accuracies for either GSPN or Simulink.

Remark that estimations for strings have a non-additive nature in comparison with single-panel estimations, as the conditions over each part of the string may differ. As such, there are many possible noises disturbing the inverter performance. In our model, this is captured by collecting input parameters for each panel that compose the string (similar to the single-panel case) and then deriving the input parameters for the entire string, based on mean and standard deviation analysis. In case the standard deviation is significant, the model can be split into the string to isolate more unstable sectors of production. Otherwise, the standard deviation may be neglected, as this is shown to be minor and will not affect the result considerably.

It remains to shown whether our dynamic model can serve for more general decision makings, in the context of a microgrid management, as follows.

## 6.2 MICROGRID MODELLING

Departing from the generator model in Fig. 12, one can now organise a plug-and-play like model that allows engineers to reconfigure and simulate specific parts of a microgrid, or vary the number and specifications of its components, such as energy sources, battery banks, and load profiles. The microgrid model proposed in this paper is shown in Fig. 16.

Model M includes 4 basic blocks, intended to design 4 different microgrid components:

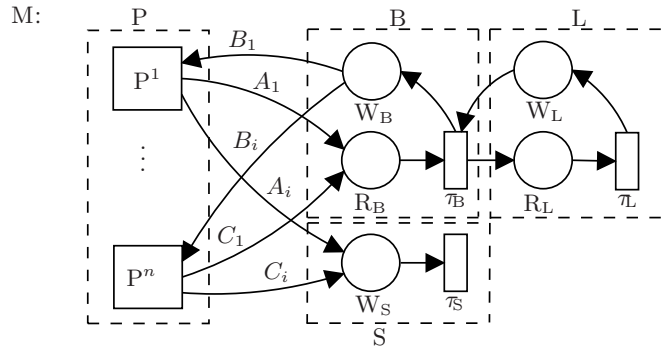


**Figure 16 – Proposed GSPN to design plug-and-play microgrid components.**

**Source: Author**

source (generator), storage (battery bank), load (consumption), and surplus (simulating the MPG interaction). The energy provided by the multiple *sources* (denoted by  $P^i$ ,  $i = 1, \dots, n$ ) are channelled either towards a *battery bank* (block B), in case it has capacity enough for charging, or towards a *surplus* resource (block S), otherwise. From block B the energy serves to a *load* simulator (block L), which represents the microgrid consumption.

Each model  $P^i$ ,  $i = 1, \dots, n$ , has a function equivalent to the model P in Fig. 12. For the storage in B, the place  $R_B$  quantifies the remaining storage level ( $\#R_B$ ), while  $\lambda_B$  defines the network rate for the block B, which is directly linked with the input of the block L. Similarly, L has a place  $R_L$  to quantify the amount of energy consumed by the microgrid ( $\#R_L$ ), while the exit point  $\lambda_L$  defines its consumption rate. Finally,  $\lambda_S$  in S models the rate of power injection into the MPG, which results from tokens inserted in the place  $W_S$  when the power generation is greater than the storage capacity.

While some parameters in M are generic, others depend on specific features collected from the infrastructure to be assessed. In the following one shows how they can be defined.

### 6.2.1 Input parameters for M

Intuitively, when the battery bank B reaches its saturation point, i.e., the symbolic amount of power carried by one token is greater than the available resources in B, the power delivered by P has to be redirected to the surplus block S. In the *on grid* mode, this represents the injection of power in the MPG, while in the *off-grid* model this means, for example, suspending generation as the saturation point has been reached.

For the purpose of modelling the power switching from B to S, guard formulas are implemented to test Boolean conditions over the arcs that connect P to B and S, as shown in

Tab. 4.

**Table 4 – Arc conditions for the microgrid model.**

Arcs	Condition
$A_1$ and $A_i$	IF((#R <sub>B</sub> ) <= 1):0 ELSE 1
$B_1$ and $B_i$	IF((#R <sub>B</sub> ) <= 1):0 ELSE 1
$C_1$ and $C_i$	IF((#R <sub>B</sub> ) <= 1):1 ELSE 0

It is also important to consider that a single microgrid may be composed of several generators, which differ in their power generation potential, delivering distinct amounts of energy to the microgrid. In terms of modelling, this means that each token may carry different values of energy, depending on where it came from. One option to address this feature is by weighting the arcs that depart from the generator according to the generator potential, i.e., each generator (or group of similar ones) delivers a distinct amount of energy to the grid. A fancier possibility is to take advantage from the *Infinity Server* property of timed transitions (see definition in Section 3) to establish customised parallel processing resources for each generator model, which will equivalently balance different power generation profiles. Therefore, let:

- #R<sub>*i*</sub> be the marking of R<sub>*i*</sub>, for each generator P<sup>*i*</sup>,  $i = 1, \dots, n$ ;
- Pt<sup>*i*</sup> be the maximum power capacity of the generator P<sup>*i*</sup> (in Watts (*W*)), such that the amount of power in M is  $Pt = \sum_{i=1}^n P^i$ ; and
- GCD( $x, y$ ) be the *Greatest Common Divisor* of the integers  $x$  and  $y$ .

Then, the parallel processing in P<sup>*i*</sup> is

$$\#R_i = \frac{Pt^i}{\text{GCD}(Pt^1, \dots, Pt^n)}. \quad (6)$$

In this way, #R<sub>*i*</sub> represents the individual impact caused by each P<sup>*i*</sup> over the microgrid potential Pt. For example, let P<sup>1</sup> and P<sup>2</sup> be two generation subsystems, such that P<sup>1</sup> includes 100 PV panels with a capacity of 350 *W* each, while P<sup>2</sup> includes 50 PV panels with a capacity of 280 *W* each.

Then,  $Pt^1 = 100 \cdot 350 = 35000W$ , and  $Pt^2 = 50 \cdot 280 = 14000W$ . By  $\text{GCD}(35000, 14000) = 7000$ , it follows that  $\#R_1 = Pt^1/7000 = 35000/7000 = 5$  and  $\#R_2 = Pt^2/7000 = 14000/7000 = 2$ . In summary, P<sup>1</sup> can process 5 tokens in parallel, which means  $5 \cdot 7000 = 35000W$  to the microgrid. Similarly, P<sup>2</sup> can process 2 tokens in parallel, which means providing  $2 \cdot 7000 = 14000W$ .

### 6.2.2 Microgrid simulations and analysis

From the model in Fig. 16, an important matter is to anticipate for engineers the variable relationship among P, B, L, and S. This may not be so easy to inform empirically or analytically, as the system variabilities cause non-addictive effects over the microgrid. Alternatively, the microgrid model in Fig. 16 can be applied over the real PV plant, simulated, and compared with the real power generation performance. Model M in Fig. 17 is a version of the model Fig. 16, adapted to represent this particular case study.

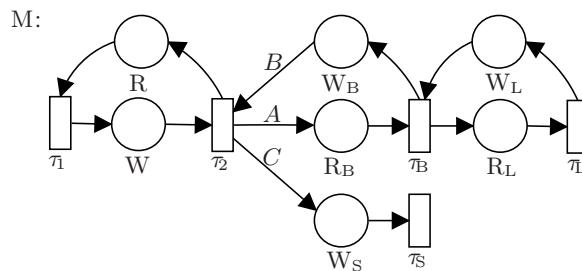


**Figure 17 – GSPN model for the case study.**

**Source: Author**

The same version of the plant is used, i.e., one inverter connected to 156 panels of  $340W$ . It delivers energy to a battery bank (place  $W_B$ ), whose capacity ( $\#R_B$ ) one aims to vary for the storage planning. The blocks L and S are also considered and used to estimate the level of consumption and surplus that result when the model M is reconfigured variably.

In the following, the focus is on anticipating the amount of energy produced by the 156 panels, considering two different scenarios: with and without microgrid consumption. Furthermore, it is considered variable sizes for the battery bank infrastructure. The following setup is assumed:

- $\#R$ : technically,  $\#R$  results from Eq. (6), i.e.,

$$\#R = \frac{156 \cdot 340}{1} = 53040W = 53kW.$$

In this experiment, only  $340W$  panels are considered. Thus,  $\text{GCD}(340) = 1$  implies that  $\#R$  may be replaced by  $\#R = 156$ , i.e., by the number of panels that compose the inverter, instead of their capacity. In this case, the semantics carried by each token means  $340W$  of power, leading to the equivalent capacity of  $340 \cdot 156 = 53040W$ . Remark that, when  $\#R = 53kW$ , each token carries  $1kW$ , while in  $\#R = 53040W$  each token means  $1W$ , and they all equivalent to design  $\#R$ .

- $\lambda_1 = 1 = \lambda_L = \lambda_S$ : for  $\lambda_1$  the same notion as in Fig. 12 is used, i.e., it is fixed to 1, so that one can vary only the time took by the panels to produce, i.e.,  $\lambda_2 \geq \lambda_1$ . Similar purpose applies for  $\lambda_L$  and  $\lambda_S$ , which are not varied;
- $\lambda_2$ : this delay is defined in Tab. 3, which includes the irradiation data that, in conjunction with the Eq. (1), allows to compute variable delays for  $\lambda_2$ . In the experiments that follow, for the sake of brevity,  $\lambda_2$  is not varied for all the intervals in Tab. 3. Instead, it is illustrated only for the solar peak, although other variations can be straightforwardly set. In this way, for the time observation of 1 hour ( $T = 1$ ), under the solar peak, it follows from Eq. (1) that

$$\lambda_2 = \frac{(1000 - 100)}{(1000 - 100)} \cdot 1 = 1.$$

In order to impose variability to the model, so that it can be measured accordingly, the following parameters are tested:

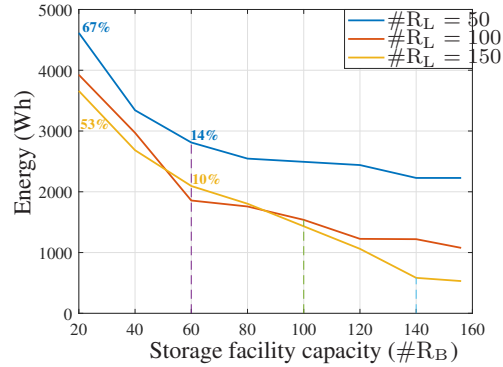
- The delay  $\lambda_B$  was varied into 1s and 0.1s, to model two profiles of power injection in  $W_L$ . Remark that the lower the delay  $\lambda_B$ , the greater the rate in L, i.e., the greater the consumption.
- The marking  $\#R_L$  was varied into 50, 100, and 150, to represent the amount of power to be absorbed in parallel by the microgrid, ranging from  $50 \cdot 340 = 17000W$  to  $150 \cdot 340 = 53040W$ .
- The marking  $\#R_B$  considers the range 20, 40, 60, 80, 100, 120, 140, and 156. This simulates variations in the storage capacity. As each token corresponds to  $340W$ , then the storage capacity ranges from  $20 \cdot 340 = 6800W$  to  $156 \cdot 340 = 53040W$ , coinciding at the upper bound with the total plant capacity.

After feeding the model with parameters, it was simulated under variability. The metrics to be estimated are the same as in equations (3) and (4), but this time applied to the place  $W_B$ , i.e., to the battery bank, which is the counterpart of the surplus  $W_S$ , so that this analysis allows to observe their behaviour under variability. The *TimeNet* setup is also the same as in section 5.1.1, and the question to be answered can be stated as follows.

**Question 2.** *For a load consumption ( $\#R_L$ ) varying from 17000W to 53040W, which is the battery bank dimensioning that accommodates the residual amount of energy left over from such a generation profile with variable load?*

Fig. 18 and Fig. 19 show possible answers provided by the model.

**Figure 18 – Storage dimensioning ( $\#R_B$ ) under three load profiles ( $\#R_L$ ): 50 to 150 tokens – 17000W to 53040W, with  $\lambda_B = 1s$ .**



In Fig. 18, the lower the load potential ( $\#R_L$ ), the greater the residual energy to be stored ( $\#R_B$ ). For example, when  $\#R_L = 50$  (low consumption profile), a storage facility of 20 tokens ( $20 \cdot 340 = 6800W$ ) would be 67% full in average, while an upgraded version of 60 tokens ( $60 \cdot 340 = 20400W$ ) would be only 14% occupied. In comparison, when  $\#R_L = 150$  (high consumption profile), the same storage facility of 20 tokens would be about 53% occupied, while the same upgrade to 60 tokens would lead to only 10% occupation.

As expected, the storage level decreasing is more substantial when  $\#R_B < \#R_L$  (before the dashed line), in which cases the consumption is higher and more tokens are moved from  $R_B$  to  $R_L$ . Otherwise, when  $\#R_B \geq \#R_L$ , more tokens are retained in  $R_B$ , and the storage level starts to stabilise.

This tendency is even more perceptible when the access to the load module L ( $\lambda_B$  in  $\tau_B$ ) is reconfigured to increase its firing rate from  $1/\lambda_B = 1s$  to  $1/\lambda_B = 0.1s$ . In practice, this means that the load profile (with the same 50, 100, and 150 parallel tokens) will now be about 10 times more frequent, which tends to consume the storage facility much faster.

As expected, Fig. 19 shows that the battery bank level decreases much faster in comparison with Fig. 18. For example, when  $\#R_L = 50$  (low consumption profile), a storage facility of 20 tokens would now be only 26% occupied, against 67% of the previous experiment. When  $\#R_L = 150$  (high consumption profile), the same storage facility of 20 tokens would be only 7% occupied, against the 50% occupation of the previous experiment. An upgrade to 60 tokens of storage ( $20400W$ ) keeps the stable 7% occupation under the high consumption rate, against the previous 14%.

Actually the entire experiment with  $\#R_L = 150$  keeps a stable storage index below

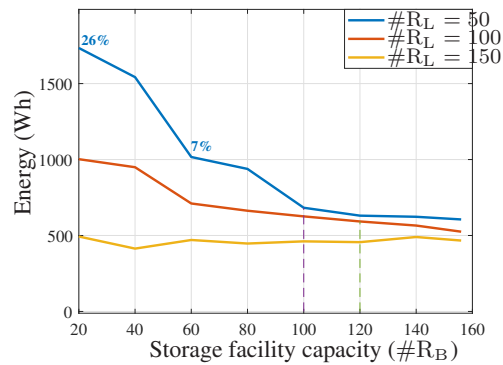


**Figure 19 – Storage dimensioning ( $\#R_B$ ) under three load profiles ( $\#R_L$ ): 50 to 150 tokens – 17000W to 53040W, with  $\lambda_B = 0.1s$ .**

10%, which means that practically the total amount of energy that will be produced, will be consumed. The other two load profiles,  $\#R_L = 100$  and  $\#R_L = 50$ , accumulate energy resources when  $\#R_B$  is less than about 100 tokens, after which the three load profiles lead to similar, stable, but very low, storage level.

There were no similar results in the literature that could be compared to ours, as we did using Simulink in Section 6.1.1. We believe this is because of the concurrent nature of microgrid components and their variabilities, which makes it hard to be reproduced by modelling and results in a large number of combinations and possible states, complexifying similar analysis.

### 6.3 EXAMPLE OF COOPERATIVE DISTRIBUTION

Consider that the evaluated PV plant is part of a larger smart grid, which delivers energy cooperatively to the main power grid, through a distribution system. The system has the following infrastructure:

- $M^1$  is a microgrid composed of 10 wind turbines of  $6kW$  each;
- $M^2$  is the evaluated PV microgrid;
- $M^3$  is a Small Hydroelectric Plant (SHP), with a potential for  $500kW$ .

For a request received from the main power grid, let us say, at 11 : 30, to deliver  $125.0kW$  for the next 1 hour, *what the prescription recommended by the system operator for dispatching those three power plants?*

Intuitively, the SHP itself can provide the total amount of power. However, water resources are always to be saved, considering their scarcity, environmental impact, and the prob-

ability of new requests in the near future. Furthermore, water uses to impose a chained effect over other plants along the course of a river, so it cannot be arbitrarily used.

Therefore, the previous question can be reintroduced this way: for a request of  $125.0kW$ , for the next 1 hour, *what would be the amount of energy produced from wind and sun resources, so that the system operator could dispatch the SHP (or other stable source) only to fulfil the remaining amount?*

Assume that a  $6kW$  turbine is capable of generating about  $3.83kW$  in an hour, with a wind incidence of, for example,  $5.4 m/s$  (this is only an assumption, as wind generation has not yet been considered in our model). Thus,  $M^1$  would be capable of delivering  $38.3kW$ . From the model, it is known that  $M^2$  delivers approximately  $42kW$ . Therefore, the remaining amount to be dispatched from  $M^3$  is  $61kW$ . This means that wind and PV units deliver approximately  $18.4\%$  and  $33.6\%$  (i.e.,  $52\%$ ) of the total request, and they act cooperatively to fulfil the expected power generation.

## 7 CONCLUSIONS AND PERSPECTIVES

In this paper, components of a PV power system are seen as event-driven entities that are modelled using GSPNs. The advantage of this approach relies on the fact that a GSPN can be simulated to anticipate performance metrics for the system, which becomes a powerful tool for engineer to plan the system, either to construct it, to expand an existing system, or to regulate energy trading contracts on the market.

The model has been tested against a real PV system. Its estimations were capable of following the real system performance with an accuracy of approximately 86%. Afterwards, the PV generation system was integrated with other components of a larger microgrid and the corresponding modelling extensions are provided. Results show that it is possible to anticipate resources planning decisions at the design time, which tends to be a valuable tool for predictive engineering in distributed power generation systems.

Future researches will focus on user interfacing and integration with generation control systems for automatic support for optimisation. Furthermore, we aim to add other types of generation profiles to the microgrid model, such as wind plants, as well as establishing new mechanisms for discovering cooperative policies for power generation systems, in the context of the cyber-physical energy grid (SUPERGRID, 2021) of the future.

## REFERENCES

ALAM, Mahamad Nabab; CHAKRABARTI, Saikat; LIANG, Xiaodong. A benchmark test system for networked microgrids. **IEEE Trans. on Industrial Informatics**, IEEE, v. 16, n. 10, p. 6217–6230, 2020.

ASMUS, Peter. Microgrids, virtual power plants and our distributed energy future. **The Electricity Journal**, Elsevier, v. 23, n. 10, p. 72–82, 2010.

BIAZARGHADIKOLAEI, Milad; SHAHABI, Majid; BARFOROUSHI, Taghi. Expansion planning of energy storages in microgrid under uncertainties and demand response. **Int. Trans. on Electrical Energy Systems**, Wiley Online Library, v. 29, n. 11, p. e12110, 2019.

CASSANDRAS, C. G.; LAFORTUNE, S. **Introduction to Discrete Event Systems**. [S.l.]: Springer Science, 2008.

CASSETTARI, Lucia; BENDATO, Ilaria; MOSCA, Marco; MOSCA, Roberto. Energy Resources Intelligent Management using on line real-time simulation: A decision support tool for sustainable manufacturing. **Applied Energy**, v. 190, p. 841–851, 2017.

CATALÃO, João PS. **Smart and sustainable power systems: operations, planning, and economics of insular electricity grids**. [S.l.]: CRC Press, 2017.

CHAMORRO, HR; ORDONEZ, CA; JIMENEZ, JF. Coordinated control based Petri Nets for Microgrids including wind farms. *In*: IEEE. **2012 IEEE Power Electronics and Machines in Wind Applications**. [S.l.], 2012. p. 1–6.

DADFAR, Sajjad; WAKIL, Karzan; KHAKSAR, Mehrdad; REZVANI, Alireza; MIVEH, Mohammad Reza; GANDOMKAR, Majid. Enhanced control strategies for a hybrid battery/photovoltaic system using FGS-PID in grid-connected mode. **Int. Journal of Hydrogen Energy**, Elsevier, v. 44, n. 29, p. 14642–14660, 2019.

DENHOLM, P.; ELA, E.; KIRBY, B.; MILLIGAN, M. **Role of Energy Storage with Renewable Electricity Generation**. [S.l.], 2010.

DESROCHERS, A. A. **Applications of Petri Nets in Manufacturing Systems: Modeling, Control and Performance Analysis**. [S.l.]: IEEE Press, 1994.

DJELLOULI, Abderrahmane; LAKDJA, Fatiha; RACHID, Meziane. Control and Management of Hybrid Renewable Energy System. *In*: SPRINGER. **Int. Conf. on Smart Innovation, Ergonomics and Applied Human Factors**. [S.l.], 2019. p. 1–10.

FAN, Yang; MING-TIAN, Fan; ZU-PING, Zhang. China mv distribution network benchmark for network integrated of renewable and distributed energy resources. *In: IEEE. China Int. Conf. on Electricity Distribution. [S.l.]*, 2010. p. 1–7.

FARHANGI, Hassan; JOOS, Geza. **Microgrid benchmarks. [S.l.]**: Wiley-IEEE Press, 2019.

GELEN, Ayetül; GELEN, Gökhan; BİÇAK, Aykut. Supervisory controller design for reactive power compensation. **European Journal of Science and Technology**, 11 2020.

GHASAEI, Arman; ZHANG, Zhi Jin; WONHAM, W Murray; IRAVANI, Reza. A Discrete-Event Supervisory Control for the AC Microgrid. **IEEE Trans. on Power Delivery**, IEEE, p. 1–1, 2020.

HARITZA, Camblong; OCTAVIAN, Curea; AITOR, Etxeberria; ALVARO, Llaría; AMÉLIE, Hacala Perret. Research experimental platforms to study microgrids issues. **Int. Journal on Interactive Design and Manufacturing (IJIDeM)**, Springer, v. 10, n. 1, p. 59–71, 2016.

HATZIARGYRIOU, Nikos; ASANO, Hiroshi; IRAVANI, Reza; MARNAY, Chris. Microgrids. **IEEE Power and Energy Magazine**, IEEE, v. 5, n. 4, p. 78–94, 2007.

IEA, International Energy Agency. **World Energy Balances: Overview. [S.l.]**, 2018. Available at: <https://shorturl.at/fuL46>. Accessed on: 01 abr. 2019.

JANA, Debashis; CHAKRABORTY, Niladri. Generalized stochastic Petri nets for uncertain renewable-based hybrid generation and load in a microgrid system. **Int. Trans. on Electrical Energy Systems**, Wiley Online Library, v. 30, n. 4, p. e12195, 2020.

KARTSON, D.; BALBO, G.; DONATELLI, S.; FRANCESCHINIS, G.; CONTE, Giuseppe. **Modelling with Generalized Stochastic Petri Nets. [S.l.]**: Wiley & Sons, 1995.

KING, D. L.; KRATOCHVIL, J. A.; BOYSON, W. E. Measuring solar spectral and angle-of-incidence effects on photovoltaic modules and solar irradiance sensors. *In: Photovoltaic Specialists Conference. [S.l.: s.n.]*, 1997. p. 1113–1116.

KOTSAMPOPOULOS, Panos; LAGOS, Dimitris; HATZIARGYRIOU, Nikos; FARUQUE, M Omar; LAUSS, Georg; NZIMAKO, Onyi; FORSYTH, Paul; STEURER, Michael; PONCI, F; MONTI, A *et al.* A benchmark system for hardware-in-the-loop testing of distributed energy resources. **IEEE Power and Energy Technology Systems Journal**, IEEE, v. 5, n. 3, p. 94–103, 2018.

LASSETER, Robert H; PIAGI, Paolo. Microgrid: A conceptual solution. *In: IEEE. Power Electronics Specialists Conference. [S.l.]*, 2004. v. 6, p. 4285–4291.

LU, Xiaoyu; ZHOU, MengChu; AMMARI, Ahmed Chiheb; JI, Jingchu. Hybrid petri nets for modeling and analysis of microgrid systems. **IEEE/CAA Journal of Automatica Sinica**, IEEE, v. 3, n. 4, p. 349–356, 2016.

MIRSAEIDI, Sohrab; SAID, Dalila Mat; MUSTAFA, Mohd Wazir; HABIBUDDIN, Mohd Hafiz; GHAFFARI, Kimia. Progress and problems in micro-grid protection schemes. **Renewable and Sustainable Energy Reviews**, Elsevier, v. 37, p. 834–839, 2014.

MURATA, T. Petri Nets: Properties, Analysis and Applications. **Proceedings of the IEEE**, IEEE, v. 77, p. 541–580, 1989.

NAVERSEN, Christian Oyn; FARAHMAND, Hossein; HELSETH, Arild; CATALÃO, João. Hydrothermal scheduling in the continuous-time framework. **ArXiv**, p. arXiv–1912, 2019.

NEHRIR, MH; WANG, Caisheng; STRUNZ, K; AKI, H; RAMAKUMAR, R; BING, J; MIAO, Zhixin; SALAMEH, Z. A review of hybrid renewable/alternative energy systems for electric power generation: Configurations, control, and applications. **IEEE Trans. on Sustainable Energy**, IEEE, v. 2, n. 4, p. 392–403, 2011.

OLIVARES, Daniel E; CAÑIZARES, Claudio A; KAZERANI, Mehrdad. A centralized energy management system for isolated microgrids. **IEEE Trans. on Smart Grid**, IEEE, v. 5, n. 4, p. 1864–1875, 2014.

PARVANIA, Masood; SCAGLIONE, Anna. Unit commitment with continuous-time generation and ramping trajectory models. **IEEE Trans. on Power Systems**, IEEE, v. 31, n. 4, p. 3169–3178, 2015.

PATHAK, Pawan Kumar; YADAV, Anil Kumar. Design of battery charging circuit through intelligent MPPT using SPV system. **Solar Energy**, Elsevier, v. 178, p. 79–89, 2019.

PAULISTA, Cássio Rangel; PEIXOTO, Túlio Almeida; RANGEL, João José de Assis. Modeling and discrete event simulation in industrial systems considering consumption and electrical energy generation. **Journal of Cleaner Production**, Elsevier, v. 224, p. 864–880, 2019.

RAMADGE, Peter JG; WONHAM, W Murray. The control of discrete event systems. **Proceedings of the IEEE**, IEEE, v. 77, n. 1, p. 81–98, 1989.

RODRÍGUEZ, Miguel Romero; DELPOUX, Romain; PIÉTRAC, Laurent; DAI, Jing; BENCHAIIB, Abdelkrim; NIEL, Eric. Supervisory control for high-voltage direct current transmission systems. **IFAC-PapersOnLine**, Elsevier, v. 50, n. 1, p. 12326–12332, 2017.

RUPNIK, Bojan; KRAGELJ, Dušan; ŠINKO, Simona; KRAMBERGER, Tomaž. Distributed Energy Resource Operation Analysis Using Discrete Event-Simulation. **Tehnički vjesnik**, Strojarški fakultet u Slavenskom Brodu; Fakultet elektrotehnike, računarstva ?, v. 27, n. 3, p. 860–867, 2020.

SALEH, Mahmoud; ESA, Yusef; MOHAMED, Ahmed. Centralized control for dc microgrid using finite state machine. *In: IEEE. Power & Energy Society Innovative Smart Grid Technologies Conference. [S.l.]*, 2017. p. 1–5.

SCHOONENBERG, Wester CH; FARID, Amro M. A dynamic model for the energy management of microgrid-enabled production systems. **Journal of Cleaner Production**, Elsevier, v. 164, p. 816–830, 2017.

SIMON, Daniel F.; TEIXEIRA, Marcelo; COSTA, Jean Patric da. Availability estimation in photovoltaic generation systems using Timed Petri Net simulation models. **Int. Journal of Electrical Power & Energy Systems**, 2021. In press.

SUPERGRID. **SuperGrid Institute: shaping power transmission**. 2021. [www.supergrid-institute.com](http://www.supergrid-institute.com).

TSAMPASIS, Eleftherios; SARAKIS, Lambros; LELIGOU, Helen; ZAHARIADIS, Theodore; GAROFALAKIS, John. Novel simulation approaches for smart grids. **Journal of Sensor and Actuator Networks**, Multidisciplinary Digital Publishing Institute, v. 5, n. 3, p. 11, 2016.

VILLALVA, Marcelo Gradella; GAZOLI, Jonas Rafael; FILHO, Ernesto Ruppert. Comprehensive approach to modeling and simulation of photovoltaic arrays. **IEEE Trans. on Power Electronics**, v. 24, n. 5, p. 1198–1208, 2009.

VIVEIROS, Carla; MELÍCIO, Rui; IGREJA, JM; MENDES, VMF. Wind energy conversion system under a supervisor deterministic finite state machine. *In: IEEE. Int. Power Electronics and Motion Control Conference. [S.l.]*, 2016.

WANG, Yujie; SUN, Zhendong; CHEN, Zonghai. Energy management strategy for battery/supercapacitor/fuel cell hybrid source vehicles based on finite state machine. **Applied Energy**, Elsevier, 2019.

ZANGENEH, Ali; MORADZADEH, Mohammad. Self-healing: Definition, Requirements, Challenges and Methods. *In: Microgrid Architectures, Control and Protection Methods. [S.l.]*: Springer, 2020.

ZHANG, Zhanqiang; DOU, Chunxia; YUE, Dong; ZHANG, Bo; LI, Fenglei. Neighbor-prediction-based networked hierarchical control in islanded microgrids. **Int. Journal of Electrical Power & Energy Systems**, Elsevier, v. 104, p. 734–743, 2019.

ZIMMERMANN, Armin; KNOKE, Michael. **TimeNET 4.0**. [S.l.], 2007. Available at: <http://www.tu-ilmenau.de/TimeNET>.

ZOKA, Y; SASAKI, H; YORINO, N; KAWAHARA, KAKK; LIU, CC. An interaction problem of distributed generators installed in a Microgrid. *In: IEEE. Int. Conf. on Electric Utility Deregulation, Restructuring and Power Technologies. Proceedings.* [S.l.], 2004. v. 2, p. 795–799.